

Gravitational wave signals of dark matter freeze-out

Danny Marfatia¹ and Po-Yan Tseng²

¹ *Department of Physics and Astronomy, University of Hawaii, Honolulu, HI 96822, USA*

² *Department of Physics and IPAP, Yonsei University, Seoul 03722, Republic of Korea*

ABSTRACT: We study the stochastic background of gravitational waves which accompany the sudden freeze-out of dark matter triggered by a cosmological first order phase transition that endows dark matter with mass. We consider models that produce the measured dark matter relic abundance via (1) bubble filtering, and (2) inflation and reheating, and show that gravitational waves from these mechanisms are detectable at future interferometers. We find that the latter model can produce a gravitational wave signal compatible with the evidence of a stochastic common-spectrum process in 12.5 years of NANOGrav data.

Contents

1	Introduction	1
2	Bubble filtering	3
3	Bubble wall velocity	4
4	Gravitational wave production	6
5	Models	6
5.1	Scalar Quartic Model	7
5.2	$SU(2)_X$ Model	9
5.2.1	Dark matter abundance	11
5.2.2	Gravitational wave signals	12
6	Summary	13

1 Introduction

The identity of dark matter (DM) and its production mechanism are among the most important open questions in physics. In the weakly interacting massive particle (WIMP) paradigm, with its thermal freeze-out mechanism, the measured DM relic density requires a WIMP mass of $\mathcal{O}(10\text{--}10^3)$ GeV, and an electroweak-scale DM annihilation cross section. The decoupling temperature T_{dec} is related to the DM mass m_χ by $T_{\text{dec}} \simeq m_\chi/24$. The vanilla version of this scenario had been challenged by the non-observation of WIMPs in DM direct detection searches. Alternative scenarios for DM production in the early universe often assume a DM sector that is out of thermal equilibrium with the standard model (SM) sector. For example, DM may be produced in the decays of a heavy particle [1, 2]. DM may also be produced by freeze-in through the feeble annihilation of particles which are thermalized with the SM bath [3–5]. However, in all of the above scenarios, the DM mass is constant during DM production.

The discovery of the 125 GeV SM-like Higgs boson h at the Large Hadron Collider (LHC) [6, 7] consolidates spontaneous symmetry breaking as the mechanism that gives the SM particles their mass. The Higgs mechanism gives the simple relation $m_f = y_f \cdot v_{\text{SM}}$ between the fermion mass m_f and its Yukawa coupling to the Higgs boson y_f , where $\langle h \rangle \equiv v_{\text{SM}} \simeq 246$ GeV is the vacuum expectation value (VEV) of the SM Higgs. A picture of the universe going through an electroweak phase transition because finite temperature effects modify its scalar potential as the universe cools down, emerges. Before the phase transition, when all the SM particles are massless, the global minimum of the scalar potential is located

at $\langle h \rangle = 0$. After the phase transition, the global minima of the potential shift to non-trivial values $\langle h \rangle \neq 0$, which gives mass to the SM particles. In the SM, the electroweak phase transition is found non-perturbatively to be a smooth crossover [8, 9]. However, since we do not fully understand the entire structure of the scalar potential of the 125 GeV Higgs boson, and since the existence of additional scalars is a possibility, the nature of the transition is unknown.

The DM mass may be generated by a similar mechanism [10–14]. The mass originates from its couplings to a scalar, which obtains a non-trivial VEV in the early universe, so that massless DM becomes massive during the phase transition. The scalar may or may not be the 125 GeV Higgs boson. We consider a first order phase transition (FOPT) in the early universe, with vacuum bubbles nucleated at temperature T_\star , which ends with the expanding bubbles populating the entire universe. The symmetric and broken phases are located outside and inside the bubbles, respectively. The massless DM particles outside the bubbles become massive when they enter the bubbles. Only massless DM particles that carry kinetic energy larger than m_χ can penetrate the bubble walls and become massive. DM inside the bubbles abruptly decouples from the thermal bath if $T_\star < T_{\text{dec}}$. The result is that the bubbles filter out a certain amount of DM and determine the DM relic abundance [13, 14]. The massless DM outside the bubbles remains thermalized with SM radiation. It is also possible that all the massless DM particles enter the bubbles after being diluted by a period of inflation, which determines the relic abundance [11]. DM particles with insufficient kinetic energy to enter the bubbles, bounce back to the symmetric phase and slow down the bubble expansion by applying pressure on the bubble walls.

The value of m_χ/T_\star needed to produce the correct DM relic abundance depends on the velocity of the bubble walls v_w . For instance, $T_\star \simeq m_\chi/30$ for $m_\chi = 1$ TeV and $v_w = 0.01$, which satisfies $T_\star < T_{\text{dec}}$. Note that DM freeze-out induced by a FOPT can easily accommodate DM masses above a PeV, which is beyond the current sensitivities of DM direct detection and LHC searches.

In this paper, we focus on gravitational wave (GW) signals of sudden DM freeze-out caused by a FOPT during which DM mass is generated. Because the power and frequency spectrum of the GW signal is model dependent, we choose two example models, *i*) Scalar Quartic Model [15–18] and *ii*) $SU(2)_X$ Model [10, 11], to demonstrate that in parameter space regions that yield the observed DM relic abundance, a detection is possible at future GW interferometers. In the Scalar Quartic Model, the DM abundance is determined by bubble filtering, while in the $SU(2)_X$ Model, the DM abundance is set by inflation and reheating.

The paper is organized as follows. Bubble filtering is described in section 2, and computations of the bubble wall velocity are detailed in section 3. In section 4, we list the contributions to GW spectra from various processes. We calculate the GW signals for the two example models in section 5, and summarize in section 6.

2 Bubble filtering

During the FOPT and bubble expansion, massless (massive) DM particles are located outside (inside) the bubble, and momentum conservation must be satisfied at the bubble wall. An incident DM particle enters the bubble if it carries kinetic energy larger than its mass inside the bubble. Otherwise, the massless DM particle is reflected and stays outside the bubble. If a thermal flux of χ is incident on the wall, the number density of DM particles that enter the bubble is [14]

$$n_\chi^{\text{in}} = n_{\bar{\chi}}^{\text{in}} \simeq \frac{g_{\text{DM}} T_\star^3}{\gamma_w v_w} \left(\frac{\gamma_w (1 - v_w) m_\chi / T_\star + 1}{4\pi^2 \gamma_w^3 (1 - v_w)^2} \right) e^{-\frac{\gamma_w (1 - v_w) m_\chi}{T_\star}}. \quad (2.1)$$

where γ_w is the Lorentz boost factor of the wall in the rest frame of the plasma, g_{DM} is the number of spin states of the DM particle, and the DM distribution has been approximated to be Boltzmann. In the non-relativistic limit, $v_w \rightarrow 0$, filtering strongly suppresses the DM number density inside the bubble as e^{-m_χ/T_\star} . In the relativistic limit, $m_\chi/(\gamma_w T_\star) \rightarrow 0$, the number density $\sim e^{-m_\chi/(2\gamma_w T_\star)}$, so there is very little filtering and n_χ^{in} approaches the equilibrium number density outside the bubble, $n_\chi^{\text{eq}}|_{T=T_\star} = g_{\text{DM}} T_\star^3/\pi^2$.

If T_\star is lower than the thermal decoupling temperature T_{dec} , the DM inside the bubble is already decoupled from the thermal bath and makes up the DM relic abundance. On the other hand, if $T_\star > T_{\text{dec}}$, the DM filtered by the bubble wall remains in thermal equilibrium and the relic abundance is determined by standard thermal freeze-out with $m_\chi/T_{\text{dec}} \simeq 24$.¹

The DM abundance today can be calculated by dividing $n_\chi^{\text{in}} + n_{\bar{\chi}}^{\text{in}}$ (at T_\star) by the entropy density $s = (2\pi^2/45)g_{\star S}T^3$, where $g_{\star S}$ is the effective number of relativistic degrees of freedom associated with entropy, and normalizing to the critical density, $\rho_c = 3H_0^2 M_{\text{pl}}^2$ [13]:

$$\Omega_{\text{DM}} h^2 \simeq 6.29 \times 10^8 \frac{m_\chi (n_\chi^{\text{in}} + n_{\bar{\chi}}^{\text{in}})}{\text{GeV}} \frac{1}{g_{\star S} T_\star^3}. \quad (2.2)$$

Using Eq. (2.1), this can be simplified to

$$\Omega_{\text{DM}} h^2 \simeq \begin{cases} 1.27 \times 10^8 \left(\frac{m_\chi}{\text{GeV}} \right) \left(\frac{g_{\text{DM}}}{g_{\star S}} \right) \left(\frac{m_\chi}{2\gamma_w T_\star} + 1 \right) e^{-\frac{m_\chi}{2\gamma_w T_\star}}, & \text{for } v_w \rightarrow 1 \\ 3.19 \times 10^7 \left(\frac{m_\chi}{\text{GeV}} \right) \left(\frac{g_{\text{DM}}}{g_{\star S}} \right) \left(\frac{1}{v_w} \right) \left(\frac{m_\chi}{T_\star} + 1 \right) e^{-\frac{m_\chi}{T_\star}}, & \text{for } v_w \rightarrow 0. \end{cases} \quad (2.3)$$

Then, $\Omega_{\text{DM}} h^2 \simeq 0.11$ requires

$$\begin{aligned} \frac{m_\chi}{2\gamma_w T_\star} - \ln \left(\frac{m_\chi}{2\gamma_w T_\star} \right) - \ln(g_{\text{DM}}) - \ln \left(\frac{m_\chi}{\text{GeV}} \right) &\simeq 16.2, & \text{for } v_w \rightarrow 1 \\ \frac{m_\chi}{T_\star} - \ln \left(\frac{m_\chi}{T_\star} \right) + \ln(v_w) &\simeq 22, & \text{for } v_w \rightarrow 0. \end{aligned} \quad (2.4)$$

For example, for $v_w \rightarrow 1$, taking $m_\chi \approx 1$ TeV and $g_{\text{DM}} = 2$, requires

$$\frac{m_\chi}{2\gamma_w T_\star} \simeq 27, \quad (2.5)$$

¹Note that even with the FOPT, T_{dec} is obtained by equating the Hubble expansion rate H and the thermal averaged DM annihilation rate, $\Gamma = \langle \sigma v \rangle n^{\text{in,eq}}$ [13]. We assume that the SM makes a dominant contribution to the light degrees of freedom so that $m_\chi/T_{\text{dec}} \simeq 24$ with logarithmic corrections that depend on m_χ , T_\star and the DM coupling.

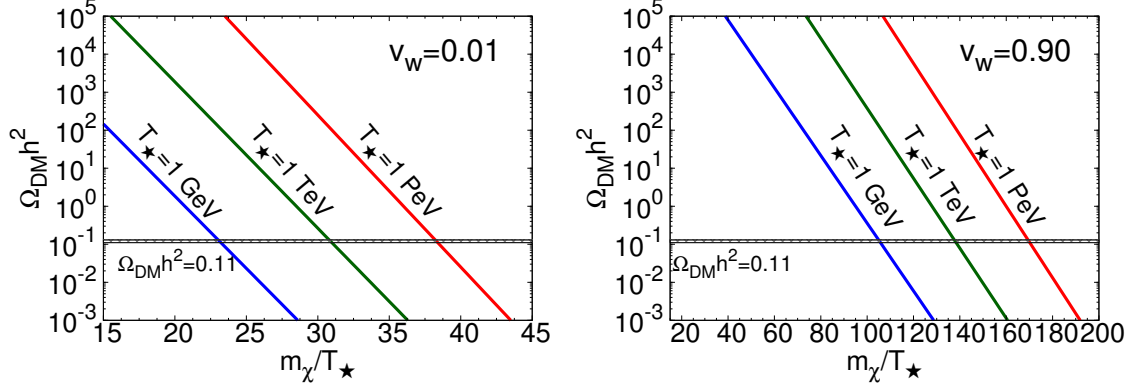


Figure 1. The DM relic abundance after bubble filtering for non-relativistic and relativistic bubble wall velocities.

to give the measured DM relic abundance, $\Omega_{\text{DM}} h^2 \simeq 0.11$.

The DM relic abundances for three values of T_\star and relativistic and non-relativistic wall velocities are shown in Fig. 1. The left-panel shows that for small v_w , $\Omega_{\text{DM}} h^2 \simeq 0.11$ if $20 \lesssim m_\chi/T_\star \lesssim 40$ and $1 \text{ GeV} \lesssim T_\star \lesssim 1 \text{ PeV}$. For $v_w \rightarrow 1$ (right panel), because bubble filtration is not efficient, larger values, $100 \lesssim m_\chi/T_\star \lesssim 170$, in the exponent of Eq. (2.1) are needed to suppress the DM number density. That larger T_\star requires larger m_χ/T_\star can be understood by combining Eq. (2.1) and (2.2): $\Omega_{\text{DM}} h^2 \propto T_\star (m_\chi/T_\star)^2 e^{-m_\chi/T_\star}$.

3 Bubble wall velocity

We consider a fermionic or bosonic DM particle χ that couples to a scalar η (that could be the SM Higgs or a new particle) with coupling g_χ (not to be confused with g_{DM} , the number of spin states). The scalar undergoes a FOPT at temperature T_\star , during which the VEV jumps from $\langle \eta \rangle = 0$ to $\langle \eta \rangle = v_\eta$. Nucleation starts at T_\star , and the bubbles expand and merge until the entire universe is populated with the v_η phase. During the bubble expansion two phases coexist. Inside the bubbles $\langle \eta \rangle = v_\eta$, and DM gets a mass $m_\chi \simeq g_\chi v_\eta$. Outside the bubbles, χ is massless because $\langle \eta \rangle = 0$. Bubble filtering occurs as described in the previous section.

DM particles that are reflected by the bubble wall exert pressure P on it, and slow down the bubble wall velocity, which is given by the equilibrium condition $\Delta V = P$, where ΔV is the potential energy difference between the false and true vacua. The strength of the phase transition is defined in terms of the latent heat of the transition,

$$\alpha \equiv \frac{(1 - T \frac{\partial}{\partial T}) \Delta V|_{T=T_\star}}{\rho_{\text{rad}}(T_\star)}, \quad (3.1)$$

where the radiation energy density, $\rho_{\text{rad}}(T) = \pi^2 g_\star T^4/30$, with g_\star the number of effectively massless degrees of freedom at temperature T . For the SM, far above the electroweak scale, $g_\star \simeq 106.75$. Note that the derivative term in Eq. (3.1) is negligible for strong, supercooled transitions, as is the case for the $SU(2)_X$ Model.

In the ultrarelativistic limit, the pressure on the bubble wall can be obtained from the difference in the number of light degrees of freedom inside and outside the bubble [14, 19, 20]:

$$P = \frac{d_n g_\star \pi^2}{90} (1 + v_w)^3 \gamma_\omega^2 T_\star^4,$$

where the ratio of the number of light degrees of freedom is

$$d_n \equiv \frac{1}{g_\star} \left[\sum_{0.2M_i > \gamma_w T_\star} \left(g_i^b + \frac{7}{8} g_i^f \right) \right],$$

with g_i^b and g_i^f , the number of degrees of freedom of the bosons and fermions, respectively. If particle i of the thermal plasma gains mass M_i inside the bubble and $0.2M_i \gtrsim \gamma_w T_\star$, then most of the i particles fail to penetrate the wall and instead exert pressure on it [14]. If i is fermionic DM with $g_{\text{DM}} = 2$, then $d_n \simeq 0.032$ including particle and antiparticle contributions. Therefore, once α is known from the scalar potential, v_w can be obtained by solving the equation, $\Delta V = P$:

$$\alpha = \frac{d_n}{3} (1 + v_w)^3 \gamma_\omega^2. \quad (3.2)$$

In the limit $v_w \rightarrow 1$, with $d_n = 0.032$, we find $\alpha \simeq 0.085 \gamma_\omega^2$ from Eq. (3.2). Eliminating γ_w from Eq. (2.5) yields the condition,

$$\frac{m_\chi}{\sqrt{\alpha} T_\star} \simeq \frac{g_\chi v_\eta}{\sqrt{\alpha} T_\star} \simeq 185, \quad (3.3)$$

to produce the measured relic abundance for $m_\chi \approx 1$ TeV. If we assume $g_\chi \simeq \mathcal{O}(1)$, a large $v_\eta/T_\star \gtrsim \mathcal{O}(10)$ and small $\alpha \lesssim \mathcal{O}(0.1)$ is required.

A precise computation of the bubble wall velocity outside the ultrarelativistic regime is beyond the scope of this paper. For bubble wall velocities faster than the speed of sound in the plasma ($1/\sqrt{3}$), but not ultrarelativistic, we use the approximation [21],

$$v_w = \frac{\frac{1}{\sqrt{3}} + \sqrt{\alpha^2 + \frac{2}{3}\alpha}}{1 + \alpha}. \quad (3.4)$$

For $v_w \rightarrow 1/\sqrt{3}$ (i.e., $\alpha \rightarrow 0$), the condition for $\Omega_{\text{DM}} h^2 = 0.11$ is

$$\frac{m_\chi}{T_\star} = \frac{g_\chi v_\eta}{T_\star} \simeq 75, \quad (3.5)$$

according to Eq. (2.1) and (2.2).

4 Gravitational wave production

A FOPT generates GWs from three processes [22]: i) Bubble collisions. ii) Sound waves in the plasma following bubble collisions and before the kinetic energy is dissipated by bubble expansion. iii) Magnetohydrodynamic (MHD) turbulence in the plasma after the bubble collisions. The GW signal is given by the linear combination of the three processes,

$$\Omega_{\text{GW}} h^2 \simeq \Omega_{\text{co}} h^2 + \Omega_{\text{sw}} h^2 + \Omega_{\text{turb}} h^2. \quad (4.1)$$

The parameters that control the signal are v_w , T_\star , the phase transition strength α , the inverse of the duration of the phase transition β/H_\star in units of the Hubble parameter at T_\star , all of which are model and scalar potential specific.

Our calculations of the GW spectra follow the semi-analytic treatment in Refs. [19, 22, 23]. Here, we simply point out some aspects of the three contributions without regurgitating the equations used. Increasing the values of T_\star and β/H_\star increases the peak GW frequency, but the latter also suppresses the power of the GW signal. The power also decreases as v_w is decreased. These properties are shared by all three GW contributions.

The GW contribution from bubble collisions can be calculated directly from the scalar field η in the envelope approximation. In this approximation, an important quantity is the fraction of latent heat transformed into scalar field gradient energy, κ_η .

GWs are produced by the sound waves created during percolation. For values of v_w not too close to the sound speed or speed of light, parametric fits to the numerically obtained GW spectrum can be found in Ref. [22]. These fits include an efficiency parameter κ_v for the fraction of latent heat transformed into bulk motion of the fluid, that depends on the expansion mode of the bubble. The peak frequency of the contribution from sound waves is inversely proportional to v_w .

The contribution from MHD turbulence arises when percolation transfers a κ_{turb} fraction of the latent heat into turbulence in the plasma. This parameter is related to κ_v via $\kappa_{\text{turb}} \simeq \epsilon \kappa_v$, where ϵ represents the fraction of bulk motion that is turbulent. The value of ϵ is still under investigation, and we conservatively take $\epsilon = 0.05$ [22], which makes the contribution from MHD turbulence small.

The values of κ_η and κ_v depend on the bubble expansion mode, and so depend on α and v_w [19]. We set $\kappa_\eta = 0$ for $\alpha \leq \alpha_\infty$, where $\alpha_\infty \simeq 4.9 \times 10^{-3} (v_\eta/T_\star)^2$, is the threshold above which the bubbles run away at the speed of light. In the case of runaway bubbles, i.e., $\alpha > \alpha_\infty$, we replace κ_v by $(\alpha_\infty/\alpha)\kappa_v$, and $\kappa_\eta = (\alpha - \alpha_\infty)/\alpha$ [22]. Consequently, for $\alpha \leq \alpha_\infty$, sound waves dominate GW production, and for $\alpha \gg \alpha_\infty$, GW production from bubble collisions is most important.

5 Models

We now investigate two example models to demonstrate that abrupt DM freeze-out produces a detectable stochastic GW background.

We consider the Scalar Quartic Model and $SU(2)_X$ Model. Both models have a quartic term as the highest order term in their scalar potentials. However, in the former model, the effective scalar potential is composed of only one scalar field η , and may be viewed as approximating a multi-field potential. There may be thermal or non-thermal contributions to the cubic term from new particles that are not heavy enough to be integrated out [16]. In this model, the DM candidate is unspecified. On the other hand, the $SU(2)_X$ Model has the SM gauge group with an extra $SU(2)_X$, and the scalar potential at the Planck scale is assumed to only permit quartic terms built from the SM scalar doublet H and a scalar doublet S under $SU(2)_X$. The absence of quadratic terms renders the model dimensionless at tree level. The quadratic terms and electroweak scale are dynamically generated [24, 25], and the $SU(2)_X$ vector bosons are automatically stable and are the DM candidates [26, 27]. A generalization of this model that includes mass terms at tree level has been studied in Ref. [28].

5.1 Scalar Quartic Model

The effective scalar potential at finite temperature is [15–18]

$$V_{\text{eff}}(\eta, T) = \frac{\mu^2 + DT^2}{2}\eta^2 - \xi T\eta^3 + \frac{\lambda}{4}\eta^4, \quad (5.1)$$

where we have neglected non-thermal contributions to the cubic term. Many particle physics models such as the inert singlet, inert doublet, and minimal supersymmetry models, can be parametrized by the above finite-temperature effective potential. Since current LHC data do not constrain the SM Higgs trilinear coupling, we may identify η with the SM Higgs, take ξ as a free parameter, and set the zero-temperature VEV to the SM value $v_\eta = v_{\text{SM}} = 246$ GeV. Then the critical temperature is [16]

$$T_c = \frac{2}{\lambda D - 2\xi^2} \left[\frac{\sqrt{\lambda D(\lambda D - 2\xi^2)T_o^2}}{2} \right], \quad (5.2)$$

where

$$T_o^2 = -\frac{\mu}{D} = \frac{\lambda}{D}v_{\text{SM}}^2, \quad (5.3)$$

is the temperature when the potential barrier vanishes. The two minima are

$$\langle \eta \rangle = 0, \quad \frac{3\xi T}{2\lambda} \left[1 + \sqrt{1 - \frac{4\lambda(\mu^2 + DT^2)}{9\xi^2 T^2}} \right] \equiv v_\eta. \quad (5.4)$$

There are three independent parameters ξ , D , and λ in the above effective potential. For simplicity, we fix $\lambda = 0.1$ in following analysis.

The nucleation temperature T_n is determined by requiring the bounce action $S_3(T_n)/T_n \simeq 142$, when the vacuum tunneling rate equals the Hubble expansion rate [15]. We adopt the following analytic approximation from Ref. [18]:

$$\frac{S_3}{T} = \frac{64\sqrt{2}\pi}{81} \frac{\xi}{\lambda^{3/2}} (2 - \delta)^{-2} (\beta_1 \delta + \beta_2 \delta^2 + \beta_3 \delta^3), \quad (5.5)$$

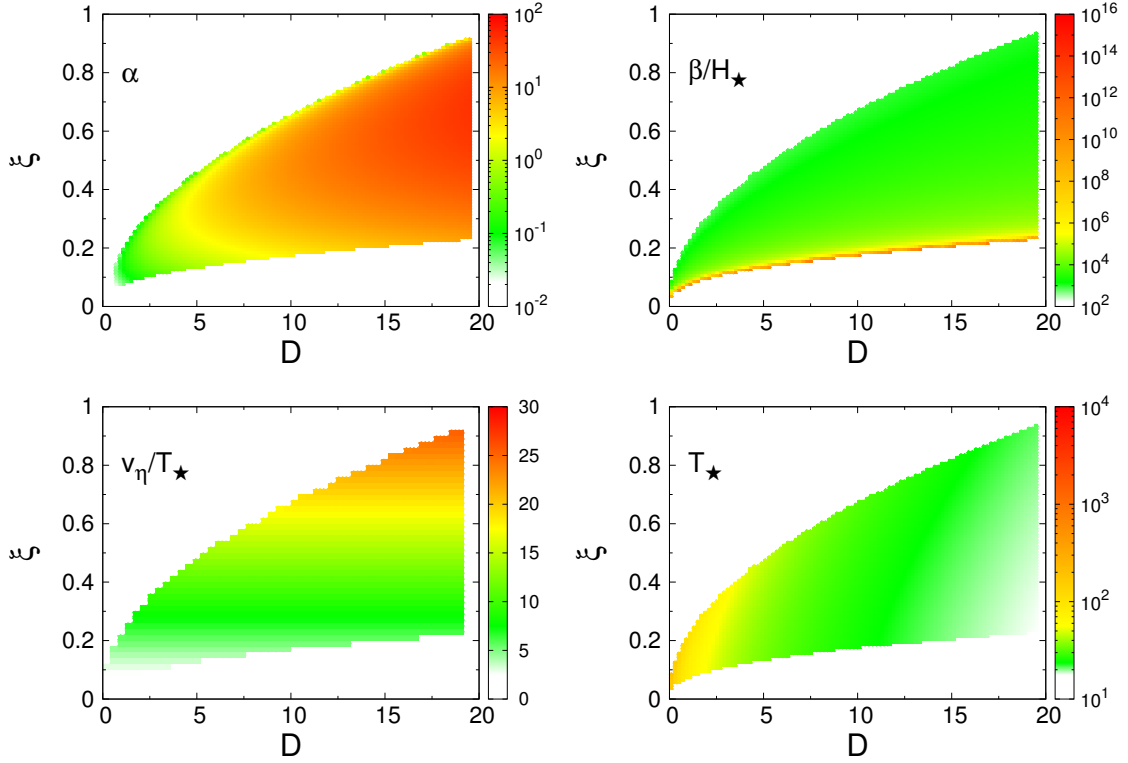


Figure 2. The parameters α , β/H_* , v_η/T_* , and T_* for the Scalar Quartic Model with $\lambda = 0.1$.

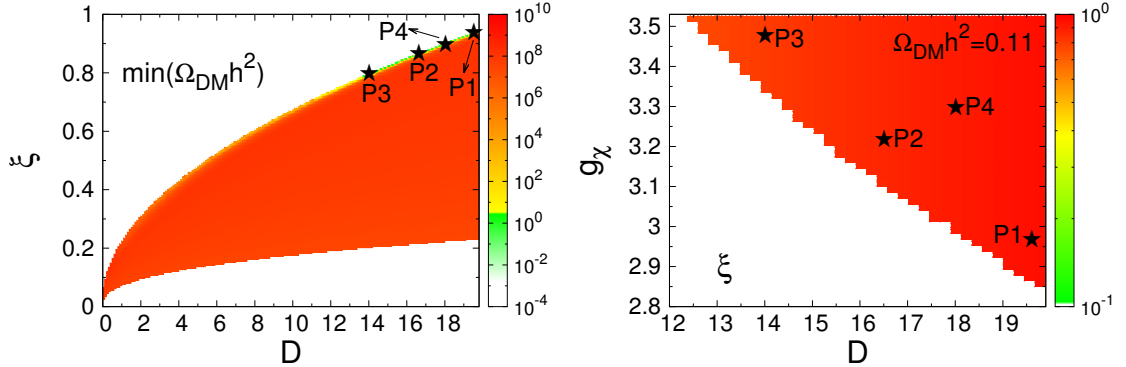


Figure 3. Scalar Quartic Model. Left: Minimal values of $\Omega_{\text{DM}} h^2$ in the (D, ξ) plane for $g_\chi \leq \sqrt{4\pi}$. Right: Values of ξ in the (D, g_χ) plane for $\Omega_{\text{DM}} h^2 = 0.11$. The stars mark the four benchmark points in Table 1.

where $\delta \equiv \lambda(\mu^2 + DT^2)/(\xi T)^2$, and $\beta_1 = 8.2983$, $\beta_2 = -5.5330$ and $\beta_3 = 0.8180$ are the results of a numerical fit. The expression is valid for $0 < \delta < 2$ which corresponds to $T_0 < T < T_c$. We choose $T_* = T_n$ to compute α and $\beta/H_* = d(S_3/T)/d(\ln T)|_{T=T_n}$ [15]. Figure 2 shows that in only narrow parameters region (for example around $(D, \xi) \simeq (18, 0.85)$), is v_η/T_* large enough (~ 25) as dictated by Eq. (3.5), to obtain the measured DM relic abundance for $g_\chi \simeq \sqrt{4\pi}$.

Table 1. Benchmark points (with $\lambda = 0.1$) for the Scalar Quartic Model that give $\Omega_{\text{DM}}h^2 = 0.11$.

	P1	P2	P3	P4
ξ	0.943	0.863	0.796	0.901
D	19.7	16.5	14.0	18.0
g_χ	2.97	3.22	3.48	3.31
α	0.089	0.082	0.076	0.121
β/H_\star	1116	1062	1015	1085
v_η/T_\star	25.71	23.41	21.49	24.51
v_w	0.768	0.763	0.760	0.791
T_\star/GeV	21.5	23.8	26.1	22.7
m_χ/GeV	1642	1799	1953	1838

The DM relic abundance is mainly determined by bubble filtering in the Scalar Quartic Model. Because of the presence of the quadratic term at tree-level, inflationary supercooling (as for the $SU(2)_X$ Model) does not occur. In the left panel of Fig. 3, we show values of the relic abundance obtained by varying D and ξ with $g_\chi \leq \sqrt{4\pi}$. In most of the parameter space DM is overproduced. However, in the narrow green region $\alpha \lesssim 0.2$; compare with the upper-left panel of Fig. 2. The values of D, ξ and g_χ for which $\Omega_{\text{DM}}h^2 = 0.11$ are displayed in the right panel of Fig. 3. The four benchmark points marked with stars in Fig. 3 are listed in Table 1.

The GW spectra for the benchmark points are shown in Fig. 4. The frequencies peak around $\mathcal{O}(10^{-3} - 10^{-2})$ Hz because $\beta/H_\star \simeq \mathcal{O}(1000)$ for all four points. This puts the model out of reach of LIGO and ET. LISA, BBO and DECIGO are sensitive to all four benchmark points because they have $\alpha \simeq 0.1$ which generates a large peak signal strength, $\Omega_{\text{GW}}h^2 \sim 10^{-12}$.

5.2 $SU(2)_X$ Model

In this dimensionless model, the SM gauge group is extended by an $SU(2)_X$ with gauge coupling g_X , and a scalar S , which transforms as a doublet under $SU(2)_X$ and is a singlet under the SM gauge group [10, 11]. The scalar potential at tree level is

$$V = \lambda_H |H|^4 - \lambda_{HS} |HS|^2 + \lambda_S |S|^4, \\ \text{where } S = \frac{1}{\sqrt{2}} \begin{pmatrix} 0 \\ \eta \end{pmatrix}, \quad H = \frac{1}{\sqrt{2}} \begin{pmatrix} 0 \\ h \end{pmatrix}. \quad (5.6)$$

$SU(2)_X$ is spontaneously broken after η acquires a VEV $\langle \eta \rangle = v_\eta$. We treat the three vector bosons of $SU(2)_X$ cumulatively as a single DM candidate with $g_{\text{DM}} = 9$ and mass $m_\chi = g_X v_\eta/2$.

In this model, as the universe cools down, the universe remains trapped in the false vacuum (i.e., $\langle \eta \rangle = \langle h \rangle = 0$) during thermal inflation due to the thermal effects. Around

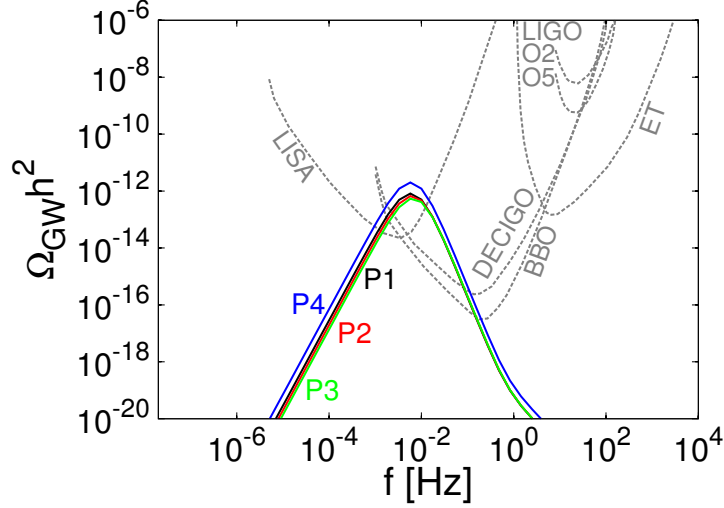


Figure 4. The GW power spectra for the four benchmark points of the Scalar Quartic Model in Table 1 and Fig. 3.

this vacuum, all particles are massless. When the energy of the false vacuum exceeds the radiation energy (i.e., $\alpha > 1$), thermal inflation begins at temperature T_{infl} with Hubble constant H_* , which are given by

$$\frac{g_* \pi^2 T_{\text{infl}}^4}{30} = \Delta V = \frac{3H_*^2 M_{\text{pl}}^2}{8\pi}. \quad (5.7)$$

During this phase, all particles undergo supercooling, because the scale factor grows exponentially and the temperature falls inversely with the scale factor. Supercooling ends at temperature T_{end} with a phase transition to the true vacuum at $\langle \eta \rangle = v_\eta$, $\langle h \rangle = v_{\text{SM}}$. Supercooling ends when the temperature falls to the nucleation temperature T_n , or earlier at the QCD phase transition temperature T_{QCD} if $T_{\text{QCD}} > T_n$:

$$T_{\text{end}} = \max(T_n, T_{\text{QCD}}), \quad T_{\text{QCD}} \simeq \frac{0.1 \langle h \rangle_{\text{QCD}}}{m_\chi / \text{TeV}}, \quad (5.8)$$

where $\langle h \rangle_{\text{QCD}} \simeq 100$ MeV. To compute the GW spectra we take $T_* = T_{\text{end}}$.

The Coleman-Weinberg mechanism generates a true minimum at $\langle \eta \rangle = v_\eta$ when the quartic λ_S becomes negative at a scale, $v_\eta e^{1/4}$ [11]. Assuming the true vacuum has zero energy, the energy in the false vacuum is $\Delta V \simeq 9m_\chi^4/(128\pi^2)$, which implies that supercooling starts at [11]

$$T_{\text{infl}} \simeq \frac{m_\chi}{8.5} \quad \text{and} \quad H_* = \sqrt{\frac{3}{\pi}} \frac{m_\chi^2}{4M_{\text{pl}}}. \quad (5.9)$$

To calculate T_n , we use the bounce action,

$$\frac{S_3}{T} = \begin{cases} \frac{873.71}{g_X^{2.37} |\ln(0.60 T/v_\eta)|}, & \text{for } g_X < 1.18 \\ 142 \times \frac{\ln(T_{\text{infl}}/v_\eta) - e^{-4.7979(g_X - 1.1779)}}{\ln(T/v_\eta)}, & \text{for } g_X \geq 1.18 \end{cases} \quad (5.10)$$

which exactly reproduces the numerical result in Fig. 1 of Ref. [11]. Nucleation occurs when $S_3(T_n)/T_n \simeq 4 \ln(M_{\text{pl}}/m_\chi) \simeq 142$.

After inflation ends, the universe is reheated by the transfer of vacuum energy ΔV from the scalars to the other particles. How quickly this occurs determines the reheating temperature T_{rh} . If the scalars decay rapidly, $T_{\text{rh}} \sim T_{\text{infl}}$, and if they oscillate and transfer energy at a rate Γ much slower than the Hubble rate before decaying, T_{rh} is lower, i.e.,

$$T_{\text{rh}} = T_{\text{infl}} \min(1, \Gamma/H)^{1/2}. \quad (5.11)$$

We assume that the energy transfer rate is dominated by Higgs decay, so $\Gamma \simeq \Gamma_h \sin^2(v_{\text{SM}}/v_\eta)$, where the Higgs decay width, $\Gamma_h \approx 4 \text{ MeV}$.

5.2.1 Dark matter abundance

Having calculated T_{infl} , T_{end} and T_{rh} , we now consider the DM relic abundance in two regimes: $T_{\text{rh}} > T_{\text{dec}}$ and $T_{\text{rh}} < T_{\text{dec}}$, where T_{dec} is the decoupling temperature in the conventional freeze-out scenario. For $T_{\text{rh}} < T_{\text{dec}}$, the DM abundance is dictated by supercooling and by sub-thermal production via scattering. Although we account for bubble filtering, its effect is negligible. On the other hand, for $T_{\text{rh}} > T_{\text{dec}}$, the supercooled population is washed out, and the sub-thermal population reattains thermal equilibrium and produces the relic abundance as in the standard freeze-out scenario. The $\Omega_{\text{DM}} h^2 = 0.11$ contour in the upper-left corner of Fig. 5 corresponds to this case.

The DM abundance resulting from inflationary supercooling is

$$\frac{n_{\text{DM}}|_{T=T_{\text{rh}}}}{s|_{T=T_{\text{rh}}}} = \frac{45g_{\text{DM}}}{2\pi^4 g_*} \frac{T_{\text{rh}}}{T_{\text{infl}}} \left(\frac{T_{\text{end}}}{T_{\text{infl}}} \right)^3 \times f_{\text{in}}, \quad (5.12)$$

where $f_{\text{in}} \equiv (n_\chi^{\text{in}}|_{T_{\text{end}}})/(n_\chi^{\text{eq}}|_{T_{\text{end}}})$ quantifies the filtering effect with $T_\star = T_{\text{end}}$ in Eq. (2.1). However, $f_{\text{in}} = 1$ for most of the parameter space of this model because the bubble wall velocity is close to the speed of light and $\gamma_w T_{\text{end}} \gg m_\chi$. The dilution from supercooling is significant for $T_{\text{infl}}/T_{\text{end}} \gg 1$, and can lead to DM being under-produced; this corresponds to the white region in the lower-right corner of Fig. 5. The DM density today can be calculated by rescaling from T_{rh} to the temperature today, 0.235 meV, and using Eq. (2.2).

We now consider sub-thermal DM production after supercooling. The decoupling temperature of this population is $T_{\text{dec}} \simeq m_\chi / \ln \lambda$, where $\lambda \equiv M_{\text{pl}} m_\chi \langle \sigma_{\text{ann}} v \rangle \sqrt{\pi g_\star / 45}$, and $\langle \sigma_{\text{ann}} v \rangle$ is the thermal averaged DM annihilation cross section of the $\text{DMDM} \rightarrow \eta\eta$ process [11]. The abundance of the sub-thermal population is obtained by solving the Boltzmann equation.

For $T_{\text{rh}} < T_{\text{dec}}$, both supercooling and sub-thermal production contribute to the DM relic abundance,

$$\Omega_{\text{DM}} h^2 = \Omega_{\text{DM}} h^2|_{\text{supercool}} + \Omega_{\text{DM}} h^2|_{\text{sub-thermal}}. \quad (5.13)$$

For $T_{\text{rh}} > T_{\text{dec}}$, the plasma thermalizes again, and the usual freeze-out mechanism yields the relic abundance,

$$\Omega_{\text{DM}} h^2 = \Omega_{\text{DM}} h^2|_{\text{freeze-out}} \simeq 0.11 \times \frac{\langle \sigma_{\text{ann}} v \rangle}{2 \times 10^{-26} \text{ cm}^3/\text{s}}. \quad (5.14)$$

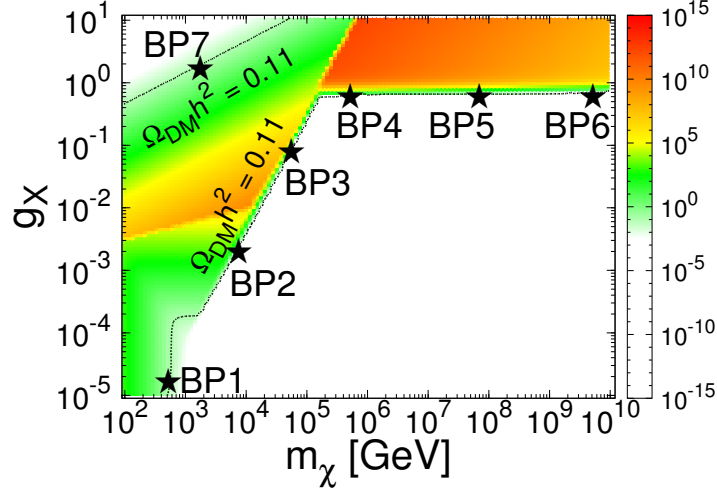


Figure 5. $\Omega_{\text{DM}}h^2$ for the $SU(2)_X$ Model with $\langle h \rangle_{\text{QCD}} = 100$ MeV. The black-dashed contours indicate the observed DM relic abundance, $\Omega_{\text{DM}}h^2 = 0.11$. The stars mark the seven benchmark points in Table 2.

Table 2. Benchmark points for the $SU(2)_X$ Model that give $\Omega_{\text{DM}}h^2 = 0.11$. Note that $T_\star = T_{\text{end}}$.

	BP1	BP2	BP3	BP4	BP5	BP6	BP7
m_χ/GeV	540	5.4×10^3	4.2×10^4	3.0×10^5	8×10^7	6×10^9	1.0×10^3
g_X	1.7×10^{-5}	1.5×10^{-3}	5.9×10^{-2}	0.72	0.77	0.82	1.4
α	1.3×10^{14}	1.2×10^{22}	1.8×10^{29}	4.4×10^{16}	2.8×10^{13}	9.4×10^{10}	4.2
β/H_\star	3.5×10^{11}	8.1×10^6	1.3×10^3	10.7	12.5	14.4	49.4
v_η/T_{end}	3.4×10^9	3.7×10^9	6.0×10^9	3.4×10^5	5.1×10^4	1.2×10^4	17.7
γ_w	2.9×10^5	2.9×10^7	1.8×10^9	1.2×10^6	2.0×10^5	4.7×10^4	123
T_\star/GeV	1.85×10^{-2}	1.87×10^{-3}	2.4×10^{-4}	2.42	4.01×10^3	1.27×10^6	82.6
T_{rh}/GeV	46.6	422	2082	3566	14.5	0.201	119

The DM relic abundance is shown in Fig. 5. We mark seven benchmark points along the dashed curves (which indicate $\Omega_{\text{DM}}h^2 \simeq 0.11$), and their values are listed in Table 2. For benchmark point **BP7**, $T_{\text{rh}} > T_{\text{dec}}$, so the DM abundance is produced by the usual thermal freeze-out. For **BP2** and **BP3** sub-thermal processes dominate. Dilution by supercooling fixes the DM abundances for **BP1**, **BP4**, **BP5**, and **BP6**. The end of supercooling occurs at the nucleation temperature for **BP4**, **BP5** and **BP6**, and at the QCD phase transition temperature for **BP1**.

5.2.2 Gravitational wave signals

To calculate the GW spectra, we need the phase transition strength α , inverse phase transition duration β/H_\star , v_w , and T_\star . We evaluate α and v_w by following the procedure of Section 3 and taking $T_\star = T_{\text{end}}$. The bounce action is used to find $\beta/H_\star \equiv d(S_3/T)/d(\ln T)|_{T=T_{\text{end}}}$. The values of these parameters are provided in Table 2 for the seven benchmark points. The points with extremely large values of α and γ_w are representative of ultra supercooling, for which the pressure P cannot counter the vacuum energy

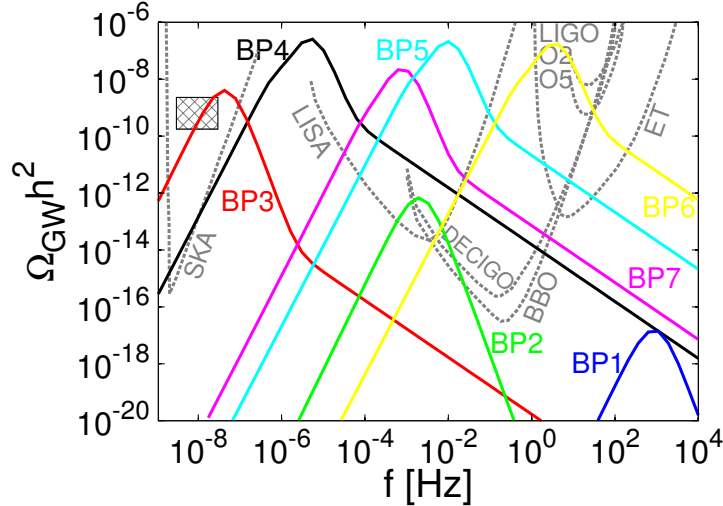


Figure 6. The GW power spectra for the seven benchmark points of the $SU(2)_X$ Model in Table 2 and Fig. 5. The signal region favored by 12.5 years of NANOGrav data [35] is shown by the hatched rectangle.

ΔV , so that bubble expansion keeps accelerating, until the bubbles collide. In the $\alpha \gg 1$ case, GWs result mainly from bubble collisions, i.e., $\kappa_\eta \simeq 1$, $\kappa_v \simeq 0$, and $\Omega_{\text{GW}} h^2 \simeq \Omega_{\text{co}} h^2$.

In Fig. 6, we display the GW spectra for the seven benchmark points and the sensitivities of the LIGO O2 and O5 observing runs [29], LISA [22, 30], ET [31], BBO [32], DECIGO [33], and SKA [34] are provided for comparison. The peak frequencies of **BP1** and **BP6** fall in the frequency range of LIGO and ET, because the large β/H_\star for **BP1** and large $T_\star \simeq 1.2$ PeV for **BP6** enhance the GW frequency from bubble collisions. However, for **BP1**, the power is suppressed by β/H_\star to an unobservable level. Signals of **BP4**, **BP5** and **BP6** can be easily detected by BBO and DECIGO. **BP4**, **BP5**, and **BP7** produce strong signals at LISA, and **BP2** is marginally detectable by LISA. Finally, **BP3** can explain the hatched rectangle signal region favored by 12.5 year NANOGrav data [35] and can produce a signal at SKA.

6 Summary

We studied the sudden freeze-out of DM as an alternative to the continuous thermal freeze-out mechanism. A necessary ingredient for sudden freeze-out is that a FOPT generates DM mass. DM mass is generated via the coupling to a scalar particle, whose potential is responsible for a FOPT. When the scalar field acquires a non-zero VEV, DM becomes massive. The DM relic abundance may be determined by bubble filtering or by inflation and reheating. Because a FOPT triggers sudden DM freeze-out, GWs offer a signature for sudden freeze-out not available for thermal freeze-out.

To assess the viability of GWs as a signal of sudden freeze-out, we considered two example models that produce a DM abundance either by bubble-filtering (Scalar Quartic

Model) or by inflation and reheating ($SU(2)_X$ Model). We showed that the observed DM relic abundance can be realized in these models with detectable GW signals in future interferometers.

In the Scalar Quartic Model, the perturbativity condition, $g_\chi \lesssim \sqrt{4\pi}$, forces the preferred parameter space to have a large $v_\eta/T_\star \gtrsim 20$ and small phase transition strength, $\alpha \lesssim 0.2$. To produce the DM relic abundance, the expanding bubbles must filter out most of the thermal DM in the symmetric phase via a large m_χ/T_\star and non-relativistic bubble wall velocity. In these parameter regions the GW spectra have peak frequencies $\mathcal{O}(10^{-2})$ Hz, and powers large enough to be probed by LISA, DECIGO, and BBO.

In the $SU(2)_X$ Model, bubble filtering has a negligible effect on the DM number density, and the DM relic abundance is governed either by supercooling during thermal inflation or sub-thermal DM production. The parameter regions that give the DM relic abundance favor $\alpha \gg 1$, which corresponds to ultra supercooling. Therefore, GWs mainly originate from bubble collisions. The GW spectra have peak frequencies that span a wide range from 10^{-7} - 10^3 Hz, and enough power to be easily probed by LISA, DECIGO, BBO and ET. For $m_\chi \geq 10^5$ GeV, the GW power can be as large as $\Omega_{\text{GW}} h^2 \simeq 10^{-7}$, which may even be detected by LIGO; see **BP6** in Fig. 6. **BP3** can explain the anomalous 12.5 year NANOGrav data [35].

Acknowledgements

D.M. is supported in part by the U.S. DOE under Grant No. de-sc0010504.

References

- [1] E. W. Kolb, D. J. H. Chung and A. Riotto, AIP Conf. Proc. **484**, no. 1, 91 (1999), [hep-ph/9810361].
- [2] R. Allahverdi, K. Dutta and A. Maharana, JCAP **1810**, 038 (2018), [arXiv:1808.02659 [astro-ph.CO]].
- [3] J. McDonald, Phys. Rev. Lett. **88**, 091304 (2002), [hep-ph/0106249].
- [4] L. J. Hall, K. Jedamzik, J. March-Russell and S. M. West, JHEP **1003**, 080 (2010), [arXiv:0911.1120 [hep-ph]].
- [5] X. Chu, Y. Mambrini, J. Quevillon and B. Zaldivar, JCAP **1401**, 034 (2014), [arXiv:1306.4677 [hep-ph]].
- [6] G. Aad *et al.* [ATLAS Collaboration], Phys. Lett. B **716**, 1 (2012), [arXiv:1207.7214 [hep-ex]].
- [7] S. Chatrchyan *et al.* [CMS Collaboration], Phys. Lett. B **716**, 30 (2012), [arXiv:1207.7235 [hep-ex]].
- [8] K. Kajantie, M. Laine, K. Rummukainen and M. E. Shaposhnikov, Nucl. Phys. B **466**, 189-258 (1996) [arXiv:hep-lat/9510020 [hep-lat]].
- [9] K. Kajantie, M. Laine, K. Rummukainen and M. E. Shaposhnikov, Phys. Rev. Lett. **77**, 2887-2890 (1996) [arXiv:hep-ph/9605288 [hep-ph]].

- [10] T. Hambye and A. Strumia, Phys. Rev. D **88**, 055022 (2013), [arXiv:1306.2329 [hep-ph]].
- [11] T. Hambye, A. Strumia and D. Teresi, JHEP **1808**, 188 (2018), [arXiv:1805.01473 [hep-ph]].
- [12] L. Heurtier and H. Partouche, Phys. Rev. D **101**, no. 4, 043527 (2020), [arXiv:1912.02828 [hep-ph]].
- [13] M. J. Baker, J. Kopp and A. J. Long, arXiv:1912.02830 [hep-ph].
- [14] D. Chway, T. H. Jung and C. S. Shin, arXiv:1912.04238 [hep-ph].
- [15] J. Kehayias and S. Profumo, JCAP **1003**, 003 (2010), [arXiv:0911.0687 [hep-ph]].
- [16] X. Wang, F. P. Huang and X. Zhang, arXiv:2003.08892 [hep-ph].
- [17] M. Dine, R. G. Leigh, P. Y. Huet, A. D. Linde and D. A. Linde, Phys. Rev. D **46**, 550 (1992), [hep-ph/9203203].
- [18] F. C. Adams, Phys. Rev. D **48**, 2800 (1993), [hep-ph/9302321].
- [19] J. R. Espinosa, T. Konstandin, J. M. No and G. Servant, JCAP **1006**, 028 (2010), [arXiv:1004.4187 [hep-ph]].
- [20] D. Bodeker and G. D. Moore, JCAP **0905** (2009) 009, [arXiv:0903.4099 [hep-ph]].
- [21] P. J. Steinhardt, Phys. Rev. D **25**, 2074 (1982).
- [22] C. Caprini *et al.*, JCAP **1604**, 001 (2016), [arXiv:1512.06239 [astro-ph.CO]].
- [23] S. J. Huber and T. Konstandin, JCAP **0809**, 022 (2008), [arXiv:0806.1828 [hep-ph]].
- [24] M. Heikinheimo, A. Racioppi, M. Raidal, C. Spethmann and K. Tuominen, Mod. Phys. Lett. A **29**, 1450077 (2014), [arXiv:1304.7006 [hep-ph]].
- [25] M. Heikinheimo, A. Racioppi, M. Raidal, C. Spethmann and K. Tuominen, Nucl. Phys. B **876**, 201 (2013), [arXiv:1305.4182 [hep-ph]].
- [26] T. Hambye, JHEP **0901**, 028 (2009), [arXiv:0811.0172 [hep-ph]].
- [27] M. Cirelli, N. Fornengo and A. Strumia, Nucl. Phys. B **753**, 178 (2006), [hep-ph/0512090].
- [28] I. Baldes and C. Garcia-Cely, JHEP **1905**, 190 (2019), [arXiv:1809.01198 [hep-ph]].
- [29] B. P. Abbott *et al.* [KAGRA and LIGO Scientific and VIRGO Collaborations], Living Rev. Rel. **21**, no. 1, 3 (2018), [arXiv:1304.0670 [gr-qc]].
- [30] P. Auclair *et al.*, arXiv:1909.00819 [astro-ph.CO].
- [31] S. Hild *et al.*, Class. Quant. Grav. **28**, 094013 (2011), [arXiv:1012.0908 [gr-qc]].
- [32] K. Yagi and N. Seto, Phys. Rev. D **83**, 044011 (2011), [arXiv:1101.3940 [astro-ph.CO]].
- [33] S. Kawamura [DECIGO working group], PoS KMI **2019**, 019 (2019).
- [34] W. Zhao, Y. Zhang, X. P. You and Z. H. Zhu, Phys. Rev. D **87**, no. 12, 124012 (2013), [arXiv:1303.6718 [astro-ph.CO]].
- [35] Z. Arzoumanian *et al.* [NANOGrav Collaboration], arXiv:2009.04496 [astro-ph.HE].